Electronic Supplementary Material (ESI) for Dalton Transactions.

Supporting information

A spectroscopic and computational study of a tough MOF with a fragile linker: Ce-UiO-66-ADC.

Alessia Airi[a], Cesare Atzori[a*], Francesca Bonino[a], Alessandro Damin[a], Sigurd Øien-Ødegaard[b], Erlend Aunan[b] and Silvia Bordiga*[a,b]

List of content:

a. *Department of Chemistry, NIS and INSTM Reference Centre, University of Torino, Via G. Quarello 15, 10135 Torino, Italy*

b. Catalysis Section, Department of Chemistry, University of Oslo, P.O. Box 1033, N-0315 Oslo, Norway

1. Materials and methods

1.1. Synthesis procedure

Cerium ammonium nitrate $(NH_4)_2Ce(NO_3)_6$ (98.5%, Sigma-Aldrich) and acetylene dicarboxylic acid H_2ADC (>90.0%, TCI chemicals) were used as purchased.
0.065 g H_2ADC were solubilized in 3.2 mL of dimethylformamide (DMF, Sigma-Aldrich) within a thick-walled glass vial, obtaining a clear solution. Then 1.06 ml of an 0.53M aqueous solution of $[(NH_4)_2[Ce(NO_3)_6]$ (previously prepared with 7.305 g in 25 mL of water) was added to the first one. After mixing, the closed vial (with a screw cap) was inserted in a preheated oven at the constant temperature of 90°C and kept in for 15 minutes. After the thermal treatment, the obtained precipitate was separated from liquid phase by centrifuge at 10 000 rpm for 5 minutes then washed with fresh DMF. The solid was washed with acetone and centrifuged for 3 times, then air dried. Same variation to the synthesis have been applied:

a. **Basic conditions**: triethylammine Et_3N (≥99%, Sigma-Aldrich) was used in order to increase the yield, the base was added to the DMF H_2ADC solution (1:1 respect to H_2ADC moles), before mixing with $(NH_4)_2Ce(NO_3)_6$ solution, obtaining a very rapid precipitation. Then the reaction mixture has been inserted in oven at 100°C for 15 minutes. The precipitate product has been isolated by centrifuge and washed as previously described.
b. **Micro-Waves assisted synthesis**: the same procedure was applied also for testing different sources of heating, introducing the same synthetic mixture in a Biotage Initiator microwave furnace for 15 minutes at 90°C under stirring the best crystalline pattern was obtained (see Figure 1 in the main text).

1.2 ^{1}H-NMR spectroscopy

Digestion NMR analysis was performed on Ce-UiO-66-ADC in order to characterize any residual solvents in the pores. The MOF (200 mg) was digested in 1M NaOD in D_2O for 10 minutes under shaking before centrifuged to separate the insoluble Ce(OD)4 from the mother liquor containing the soluble organic species. The mother liquor was analyzed using NMR spectroscopy (Bruker AVII 400, 128 scans, d1=5 sec). The NMR analysis confirmed the presence of DMF (both from DMF itself, and from its decomposition products: formate and dimethylamine). No linker was observed, as expected as it contains no protons.

1.3. Electron Microscopies

SEM: the micrographs were collected using a Zeiss Evo 50 xvp microscope equipped with a LaB_6 crystal electron source working at 20 kV of accelerating potential. The sample had been previously coated in gold by sputter deposition.

TEM: the micrographs were collected using a TEM JEOL JEM 3010 UHR microscope equipped with a LaB_6 electron source working at 300 kV of accelerating potential and a EDS OXFORD energy dispersion detector (0,17 nm of theoretical resolution). The images have been collected by a CCD

camera Gatan, Model 894 US1000 (2k x 2k). The sample has been prepared depositing a small amount of powder over a 200 mesh lacey carbon copper screen.

1.4. PXRD

The sample was placed in a 0.7 mm Ø glass capillary, and PXRD patterns in the range of 2θ = 4°-70° were acquired over 24 hours on a Bruker D8 Advance diffractometer with Cu K-α radiation.
VTXRD: Diffraction patterns have been collected with a PW3050/60 X'Pert PRO MPD diffractometer, working in Bragg-Brentano geometry, using Cu anode.
Non-ambient chamber Anton Paar XRK900 with Be windows was used to collect the PXRD data in dynamic vacuum, with ramp rate of 2°C/min. Each 2θ scan was collected every 10° C, rising in temperature from RT to 190°C.

1.5. DR-UV-vis spectroscopy

Ce-UiO-66-ADC spectra have been collected with a Varian Cary 5000 UV-vis-NIR spectrophotometer working in diffuse reflectance mode in the 200-2500 nm, with resolution of 1 nm.
H2ADC and [(NH4)2[Ce(NO3)6] aqueous solutions spectra have been collected in transmission mode in spectral range of 200-800 nm with a resolution of 1 nm.

1.6. Thermo Gravimetric Analysis

The thermo-gravimetric analysis (TGA) has been conducted using a TA Instruments Q600 programmed for rising 3°C/min from RT to 700°C in both air and N_2 atmosphere (100 mL/min flows), on about 10 mg of each sample in an alumina crucible.

1.7. 77K N_2 adsorption

Adsorption measurements were performed on a Micromeritics ASAP 2020 apparatus working at 77K with about 40 mg of sample.

1.8. FT-IR spectroscopy

Infra-red spectra have been collected by Thermo Scientific Nicolet 6700 FTIR spectrometer equipped with a HgCdTe detector in transmission mode using a self-supporting pellet in the range 400-4000 cm-1 with a resolution of 2 cm^{-1}.

1.9. Raman Spectroscopy

Raman spectra of a self-supporting pellet of sample activated at different temperatures, were collected with a Renishaw InVia Raman microscope working with a 785 nm laser diode and a 20X objective, accumulating for 20 seconds with 1 mW laser power in the 3200-100 cm^{-1} Raman shift range. Spectra of powdered material were collected using 785 nm, 514 nm (Ar^+ laser) and 442 nm (He-Cd lasers) exciting laser lines: spectra result from 10 acquisitions each one of 20 seconds. Power at the sample was maintained below 1 mW. In order to reduce the risk of thermal degradation, a special setup providing the sample rotation under the laser beam has been adopted.[1]

2. Detection of terminal alkyne

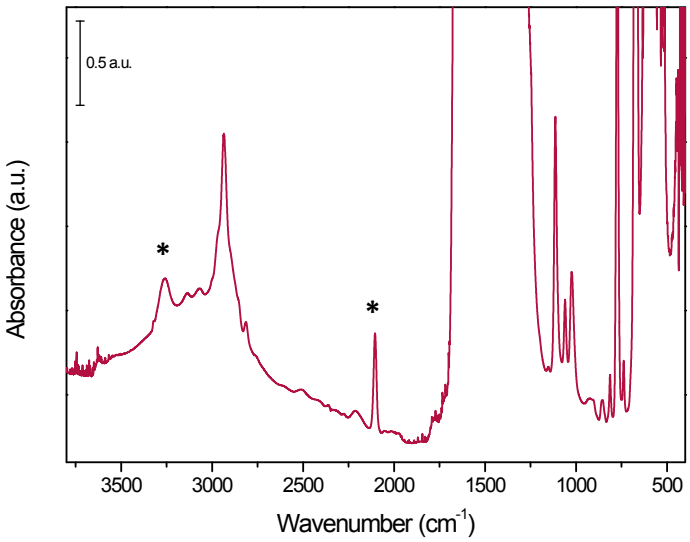

Figure S1 FT-IR spectrum of 90°C in vacuum outgassed material.

The IR spectrum was collected on the activated sample (high vacuum overnight at 90°C) in order to minimize interferences due to adsorbed molecules. The spectrum is characterized by the presence of a signal at 3260 cm^{-1} and a strong sharp band at 2107 cm^{-1} which can be easily attributed to a terminal alkyne, compatible with the decarboxylation product of the linker, see Scheme 1 in main text.

3. Structure and morphology description

3.1. Influence of Et_3N. PXRD

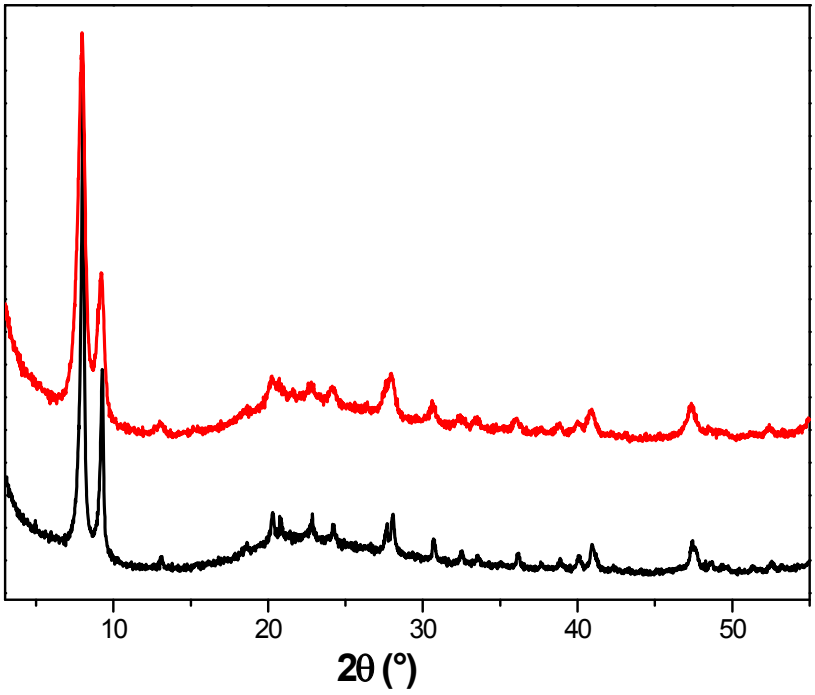

Figure S2. PXRD patterns of Ce-UiO-66-ADC. Sample obtained without the use of Et_3N (black line); sample obtained in presence of Et_3N (red line).

The two materials present the same pattern. None significant differences are visible except for the width of reflexes, due to the faster precipitation in presence of Et_3N, which produce smaller crystal domains.

By the comparison of the PXRD patterns it is possible to affirm that the different synthetic procedures applied result to produce the same crystal phase, denoted as Ce-UiO-66-ADC.

3.2. SEM microscopy

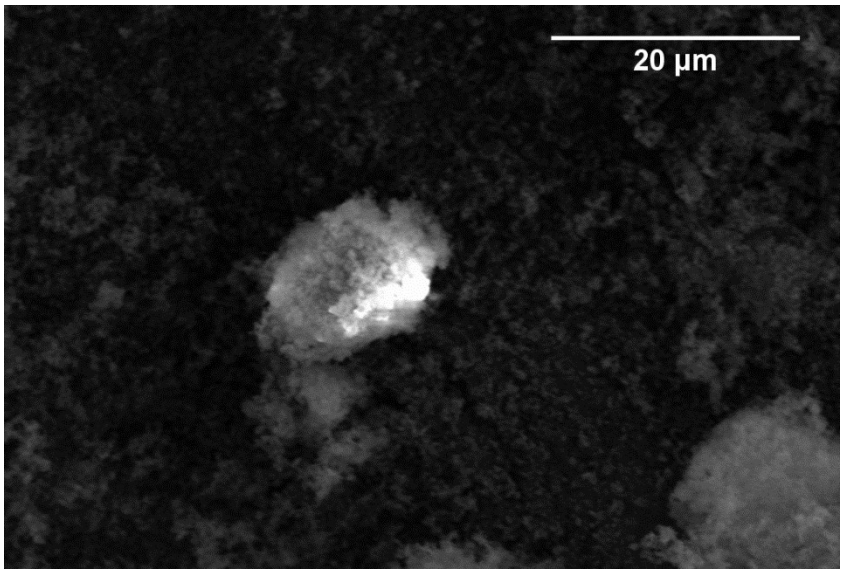

Figure S3. SEM images of Ce-UiO-66-ADC (synthetized in basic conditions).

3.3. TEM microscopy

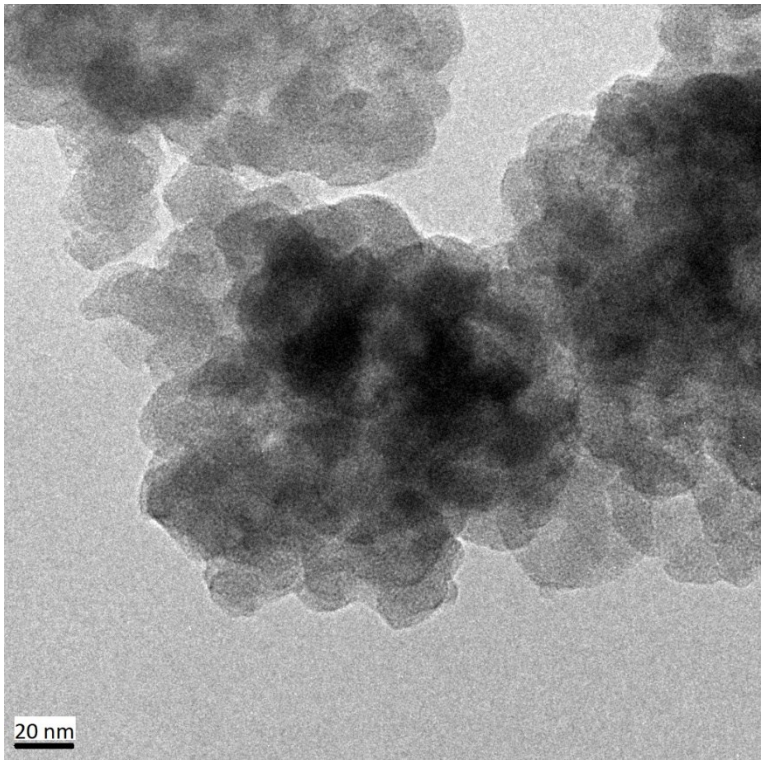

Figure S4. TEM images of Ce-UiO-66-ADC (synthetized in basic conditions).

3.4. Structure

Using cell parameters obtained from a Pawley fit (FM-3m, a = 19.11 Å), a model based on 12-connected clusters, containing 6 Ce atoms, was constructed in Materials Studio v8 (Biovia, 2019), and geometrically optimized with the Forcite program. This model was used in a Riedveld refinement (using 2θ 4°-65°) where the Ce position was allowed to refine, leading to the structure reported herein.

This is the output file of the refinement:

Chemical formula: $[Ce_6O_4(OH)_4(ADC)_6]$

R-Values

```
Rexp : 6.78     Rwp : 9.67      Rp  : 7.38   GOF : 1.43
Rexp`: 16.65    Rwp`: 23.75     Rp` : 24.03  DW  : 1.03
```

Quantitative Analysis - Rietveld

```
   Phase 1  : ""                              100.000 %
```

Background

```
   Chebychev polynomial, Coefficient  0      188.3758
                                      1      -140.7667
                                      2      100.135
                                      3      -54.67057
                                      4      40.87468
                                      5      -37.97169
                                      6      30.43907
                                      7      -4.02601
                                      8      -11.60408
                                      9      10.07483
                                      10     -9.637173
```

Instrument

```
   Primary radius (mm)                        166
   Secondary radius (mm)                      209
   Simple axial model (mm)                    7.688171
```

Corrections

```
   Zero error                                 0.01658058
   LP Factor                                  27.3
```

Structure 1

```
   Phase name
   R-Bragg                                    3.525
   Spacegroup                                 FM-3M
   Scale                                        3.03507e-007
   Cell Mass                                  6563.734
   Cell Volume (Å^3)                          6978.94642
   Wt% - Rietveld                             100.000
   Double-Voigt|Approach
      Cry size Lorentzian                     108.1
      k:  1  LVol-IB (nm)                     68.847
      k:  0.89  LVol-FWHM (nm)                96.248
```

Strain	
Strain L	1.188662
Strain G	0.0001
e0	0.00259
Crystal Linear Absorption Coeff. (1/cm)	300.588
Crystal Density (g/cm^3)	1.562
Lattice parameters	
a (Å)	19.1101144

Site	Np	x	y	z	Atom	Occ	Beq
Ce1	24	0.13662	0.00000	0.00000	Ce	1	0
O2	32	0.06392	0.06392	0.06392	O	1	0
C3	48	0.16710	0.16710	0.00000	C	1	0
C4	48	0.22598	0.22598	0.00000	C	1	0
O5	96	0.18582	0.10019	0.00000	O	1	0

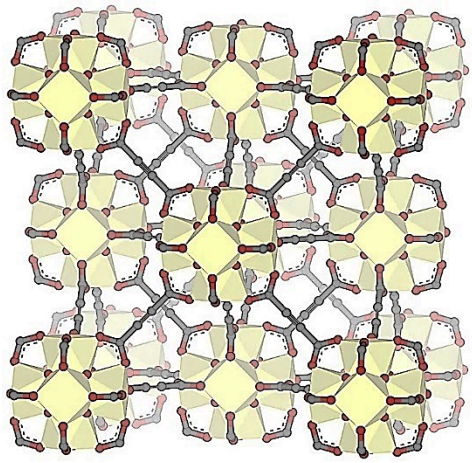

Figure S5. Elementary cell of Ce-UiO-66-ADC

4. DFT calculations

Periodic DFT[2] based calculations were performed by exploiting the hybrid B3LYP[3,4] functional and the empirical D3(BJ)[5–7] scheme for the description of dispersive interactions and including the Axilrod-Teller-Muto type three-body term. In the whole set of calculations, the CRYSTAL software[8,9] package was employed: this allows a complete treatment of periodic systems through the use of atom-centred linear combinations of Gaussian type functions for the description of atomic orbitals (basis set). Basis set adopted in present calculations is below described:

a) Ce inner electrons (28) were replaced by an effective core potential (ECP), the remaining 30 electrons being explicitly treated through a (10sp7d8f)/[4sp2d3f] basis set. The same scheme was already employed in Ref[10] for Ce description in CeO_2 and Ce_2O_3 systems. See also http://www.crystal.unito.it/basis-sets.php.

b) O and C atoms were described through a (8s6sp2d)/[1s3sp2d] and (6s5sp2d)/[1s3sp2d] all-electron basis sets respectively. They were obtained by ones employed in Ref[11], simply by splitting the original d shell through an even tempered recipe. For their full description see also Table S2.

c) For H atoms the adopted all electron basis set was a (7s1p)/[3s1p]] one already adopted in Ref[12]. See also http://www.crystal.unito.it/basis-sets.php.

Numerical accuracy in energy calculation were determined by setting thresholds for mono- and bi-electronic integral to {1188836} through the keyword (TOLINTEG). Shrinking factor parameter (keyword SHRINK), determining the k-points sampling in the reciprocal space, was set to 3 (corresponding to 4 irreducible k points). The defaults values for all the unreported computational parameters concerning the structure optimization, frequency and the associated Raman intensities calculation were used.

O (8s6sp2d)/[1s3sp2d] basis set	C (6s5sp2d)/[1s3sp2d] basis set
8 6	6 6
0 0 8 2 1.0	**0 0 6 2 1.0**
8020. 0.001080	4563.24000 0.00196665
1338. 0.008040	682.02400 0.01523060
255.4 0.053240	154.97300 0.07612690
69.22 0.168100	44.45530 0.26080100
23.90 0.358100	13.02900 0.61646200
9.264 0.385500	1.82773 0.22100000
3.851 0.146800	**0 1 3 4 1.0**
1.212 0.072800	20.96420 0.11466000 0.04024870
0 1 4 6 1.0	4.80331 0.91999900 0.23759400
49.43 -0.008830 0.009580	1.45933 -0.00303068 0.81585400
10.47 -0.091500 0.069600	**0 1 1 0 1.0**
3.235 -0.040200 0.206500	0.483456 1. 1.
1.217 0.379000 0.347000	**0 1 1 0 1.0**
0 1 1 0 1.0	0.145585 1. 1.
0.486 1. 1.	**0 3 1 0 1.0**
0 1 1 0 1.0	1.6 1.
0.1925 1. 1.	**0 3 1 0 1.**
0 3 1 0 1.	0.4 1.
1.6 1.	
0 3 1 0 1.	
0.4 1.	

Table S1: Gaussian basis sets (reported in the CRYSTAL code format) adopted in present calculations for the description of O and C atoms.

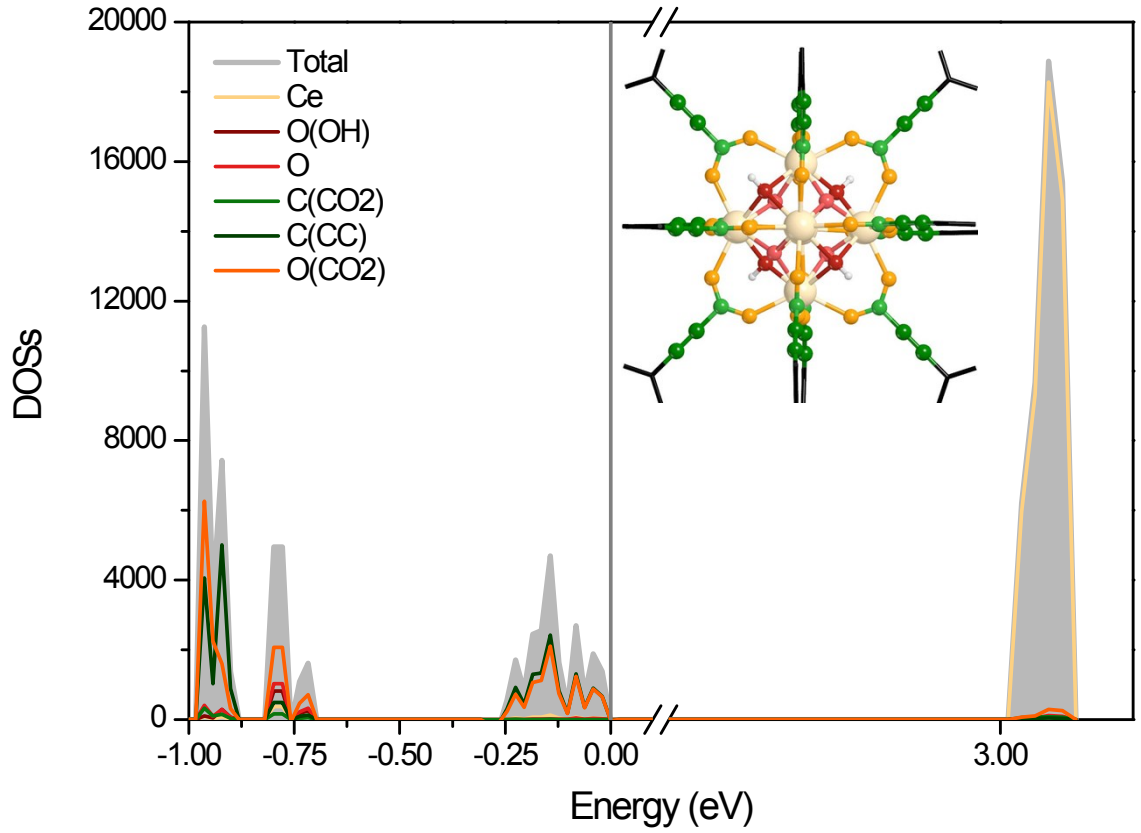

Figure S6. Total density of states (filled grey curve) computed on optimized Ce-UiO-66-ADC structure. Contributions from different atomic species (solid lines) constituting the repeating unit of Ce-UiO-66-ADC (see inset for a graphical representation) are also reported for the sake of comparison.

5. UV-vis spectroscopy

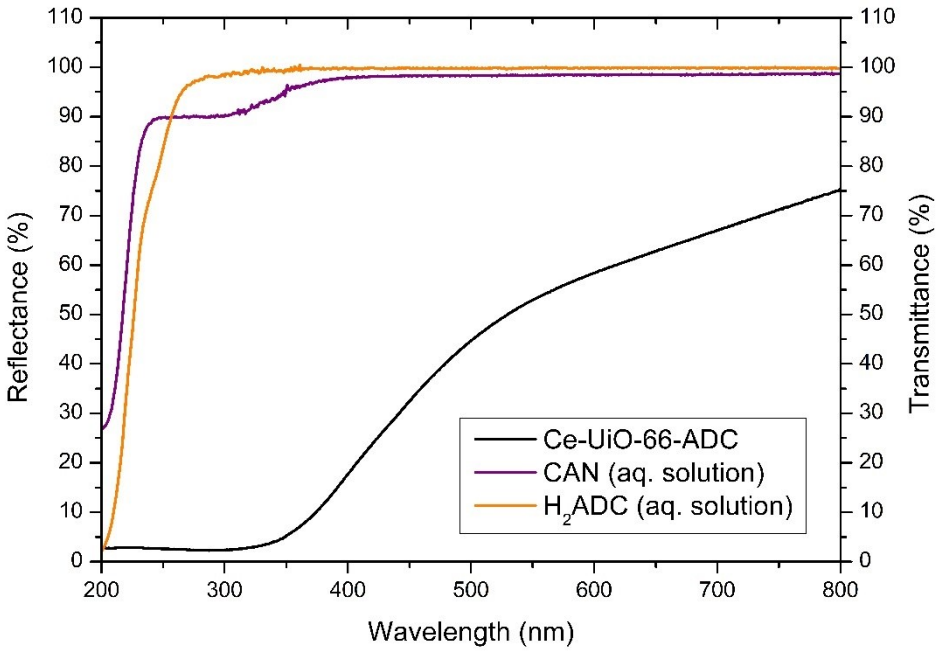

Figure S7. DR-UV-vis spectrum of Ce-UiO-66-ADC (black), compared with transmission UV-vis spectra of the solubilized precursors H_2ADC (orange) and Cerium ammonium nitrate CAN (violet).

As shown in Figure S7, the Ce-UiO-66-ADC UV-vis spectrum results to be more complex than the simply sum of the two spectra of its precursors, suggesting a deep change in the electronic structure with the formation of the solid.

6. Thermal stability

6.1. VTXRD

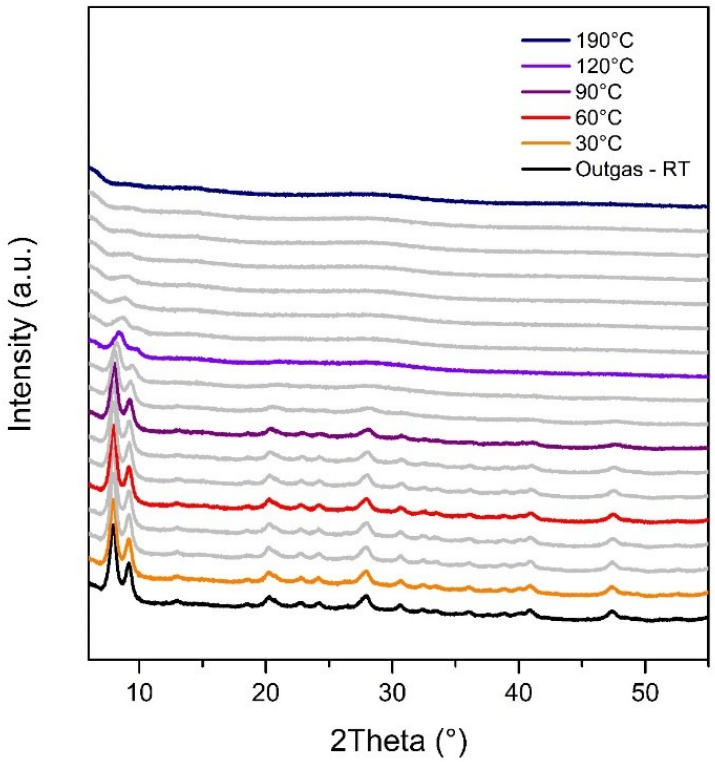

Figure S8. Ce-UiO-66-ADC PXRD patterns from RT (bottom) to 190°C (top) rising 10° per step. The colours underline the temperature selected for activation in following measurements (same colour code).

6.2. TGA

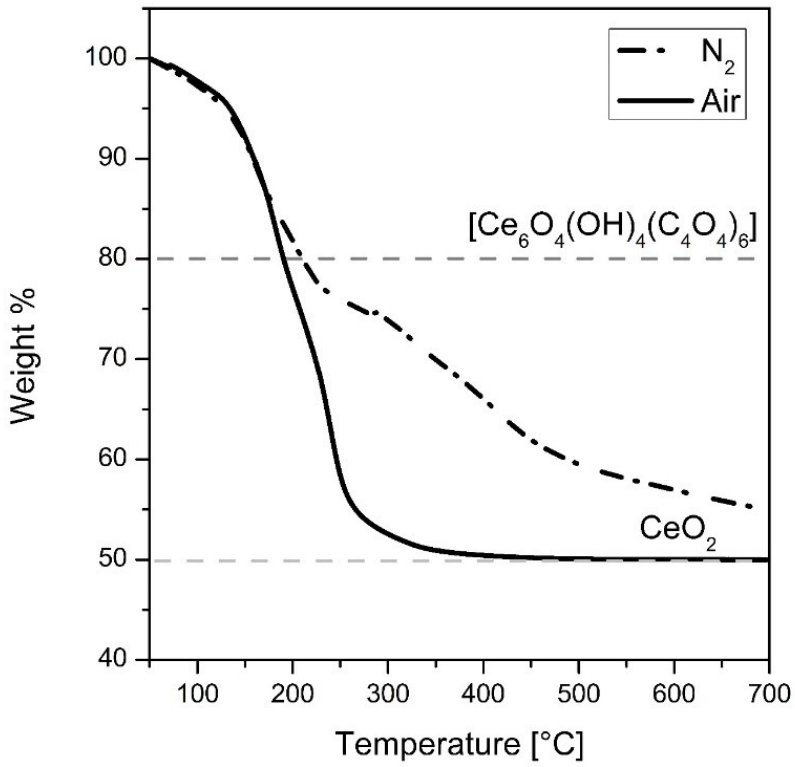

Figure S9. TGA curves of Ce-UiO-66-ADC, under dry air (solid line) and in N_2 (dot line) flux.

7. Specific surface area

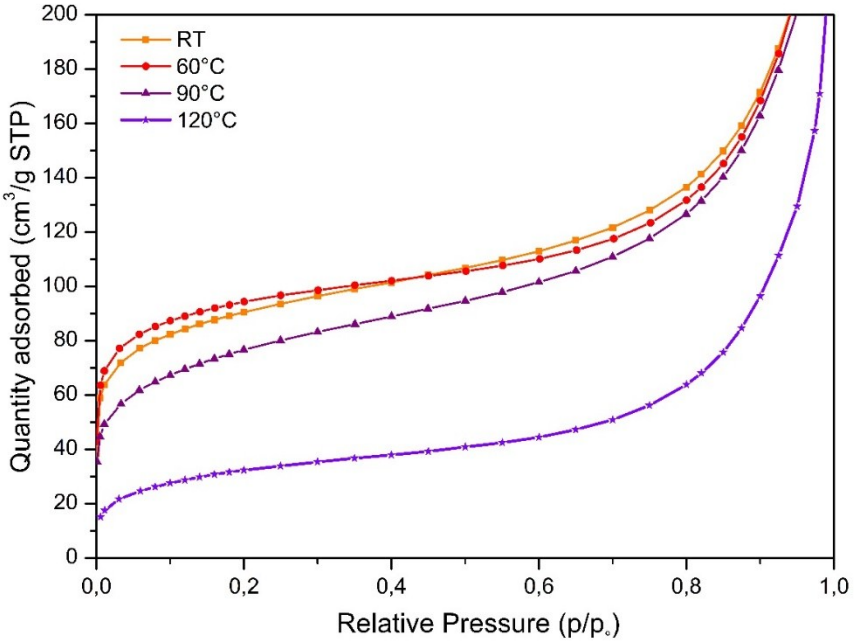

Figure S10. N_2 adsorption 77K isotherms for sample activated at different temperatures.

Outgassing Temperature (°C)	Langmuir Surface area (m^2/g)	B.E.T. surface area (m^2/g)
RT	425 ± 5	326 ± 2
60	437 ± 4	345 ± 2
90	371 ± 6	273 ± 2
120	163 ± 3	118 ± 1

Table S2. Specific surface area values after in vacuum thermal outgassing.

Theoretical Specific Surface Area:

N_2 accessible surface area was estimated using both a crude geometrical summation of the Connolly surface, and a simulated adsorption isotherm calculated using the Sorption module in Materials Studio. Surface calculation gave a result of 1131 m^2/g, whereas the simulated sorption isotherm gave a BET surface area of 889 m^2/g using the pressure range of $p/p_0 = 0.00031 – 0.01755$.

8. Raman spectrum analysis and bands assignment

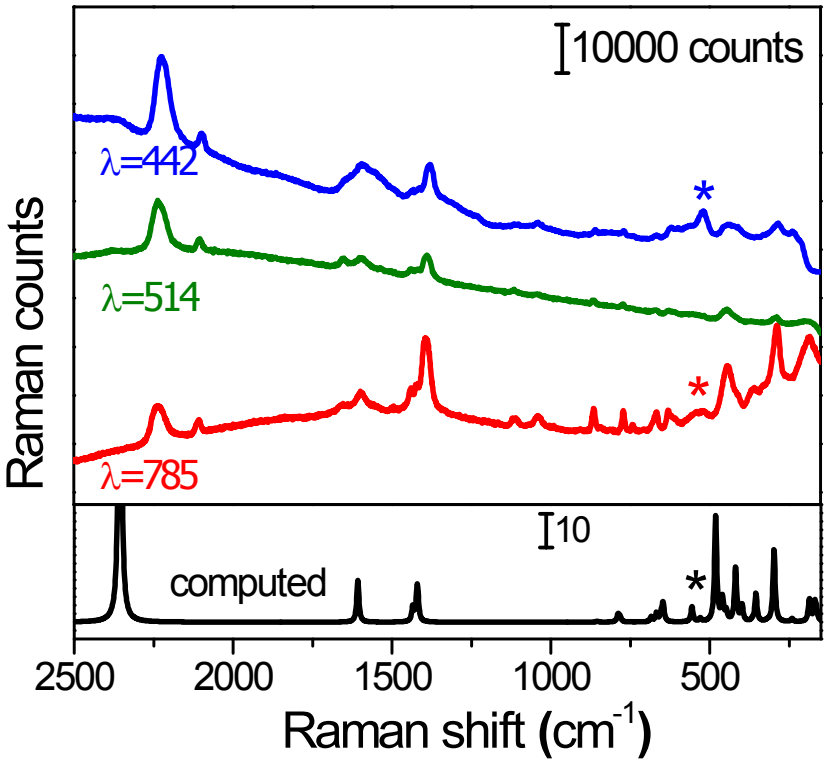

Figure S11. Raman spectra collected with different wavelength of irradiation (blue line: 442 nm, green: 514 nm, red: 785nm) in the Raman shift range between 2500 and 250 cm^{-1}, compared with the computed one (black line).

The Raman spectrum of Ce-UiO-66-ADC is characterized by three main regions, starting from higher wavenumbers: 2200-2100 cm^{-1} C≡C stretching region; 1600-1380 cm^{-1} carboxylate stretching region; below 1000 cm^{-1} are present the complex modes of the metal-oxide cluster. The Raman spectrum collected with the λ=785 nm laser shows also the fingerprints of DMF: maxima observed at 773, 864 ,1030, 1120 cm^{-1}.

The complete assignation of the Raman active modes of Ce-UiO-66-ADC is reported in Table S3.

Experimental (cm^{-1})	Computed (cm^{-1})	Moiety	Description
2235	2337	linker	R-(C≡C)-R stretching
2107	-	defective linker	R-(C≡C)-H stretching
1594	1592	linker	(COO^-) asymm stretching
1391	1416	linker	(COO^-) symm stretching
741	802	linker	COO^- out of plane
665	656	cluster+ linker	O-H bending + C-(COO-) bending
622	644	cluster+ linker	O-H bending + COO- bending
521	556	cluster	Ce-O
440	482	cluster + linker	Ce-O(COO^-) symm stretching
418	412	cluster	Ce-O breathing symm
359	355	cluster + linker	Ce-O breathing asym + out of plane C-$(COO)^-$
285	302	cluster + linker	Ce-O(COO^-) asymm
205-150	184,162	cluster + linker	Coupled complex modes of Ce-O(COO^-)

Table S3. Frequencies of the principal Raman active vibrational modes of Ce-UiO-66-ADC.

REFERENCES:

1 M. Signorile, F. Bonino, A. Damin and S. Bordiga, *Top. Catal.*, 2018, **61**, 1491–1498.

2 P. Hohenberg and W. Kohn, *Phys. Rev.*, 1964, **136**, B864–B871.

3 A. D. Becke, *J. Chem. Phys.*, 1993, **98**, 1372–1377.

4 C. Lee, W. Yang and R. G. Parr, *Phys. Rev. B*, 1988, **37**, 785–789.

5 S. Grimme, J. Antony, S. Ehrlich and H. Krieg, *J. Chem. Phys.*, 2010, **132**, 154104.

6 S. Grimme, S. Ehrlich and L. Goerigk, *J. Comput. Chem.*, 2011, **32**, 1456–1465.

7 S. Grimme, A. Hansen, J. G. Brandenburg and C. Bannwarth, *Chem. Rev.*, 2016, **116**, 5105–5154.

8 R. Dovesi, A. Erba, R. Orlando, C. M. Zicovich-Wilson, B. Civalleri, L. Maschio, M. Rérat, S. Casassa, J. Baima, S. Salustro and B. Kirtman, *Wiley Interdiscip. Rev. Comput. Mol. Sci.*, 2018, **8**, 1–36.

9 R. Dovesi, V.R. Saunders, C. Roetti, R. Orlando, C. M. Zicovich-Wilson, F. Pascale, B. Civalleri, K. Doll, N.M. Harrison, I.J. Bush, Ph. D'Arco, M. Llunel, M. Causà, Y. Noel, L. Maschio, A. Erba, M. Rérat, S. Casassa, CRYSTAL17 User's Manual, 2018.

10 J. Graciani, A. M. Márquez, J. J. Plata, Y. Ortega, N. C. Hernández, A. Meyer, C. M. Zicovich-Wilson and J. F. Sanz, *J. Chem. Theory Comput.*, 2011, **7**, 56–65.

11 L. Valenzano, B. Civalleri, S. Chavan, S. Bordiga, M. H. Nilsen, S. Jakobsen, K. P. Lillerud and C. Lamberti, *Chem. Mater.*, 2011, **23**, 1700–1718.

12 R. Dovesi, C. Ermondi, E. Ferrero, C. Pisani and C. Roetti, *Phys. Rev. B*, 1984, **29**, 3591–3600.